

THE INTERNATIONAL JOURNAL OF SCIENCE & TECHNOLEDGE

Aerosol Optical Depth and Precipitation Rate Projections over East Africa Utilizing Self Organizing Map

John Wanjala Makokha

Lecturer, Department of Science Technology and Engineering, Kibabii University, Kenya

Hudson K. Angeyo

Senior Lecturer, Department of Physics, University of Nairobi, Kenya

John N. Muthama

Professor, Department of Meteorology, University of Nairobi, Kenya

Abstract:

Assessment of future aerosols impacts on both regional and global climate change requires a comprehensive projection tool that reliably provides information on aerosol evolution characteristics with high fidelity. In the current study, we propose an algorithm based on Self-Organizing Map (SOM) and Community Atmosphere Model 4 (CAM4) for long term Aerosol Optical Depth (AOD) and Precipitation Rate (PR) projections over East Africa. To start with, AOD and PR retrievals from Moderate Resolution Imaging Spectroradiometer (MODIS) and Tropical Rainfall Measurement Mission (TRMM) respectively were cross validated with simulation from CAM4 so as to assess the uncertainty between the measured and simulated retrievals from 2000 to 2014. The error analysis between CAM4 simulations and MODIS measurements (from 2000 to 2014) shows a close match where R^2 varies from 0.58 to 0.83 with a corresponding RMSE of between 0.014 and 0.065 (for AOD). Likewise, the uncertainty between simulated and measured PR from CAM4 and TRMM showed an estimated R^2 to range between 0.40 and 0.78 while the RMSE varied from 0.021 to 0.091 in the same period and study sites. Based on proposed SOM algorithm and simulated CAM4 retrievals over each study site, an increase of between 1.34-2.43 % for AOD and a decrease of between 1.03-1.98 % in PR are projected over the region by 2030.

Keywords: East Africa, self-organizing map, projections, spatial and temporal analysis, aerosol optical depth, precipitation rate

1. Introduction

Extraction of aerosol optical properties and characteristic patterns of variability from a large data set is vital to correctly monitor atmospheric processes in relation to climate change (Liu and Weisberg, 2005). Therefore, techniques for pattern detection i.e. clustering, classifying and feature extraction in multispectral imaging datasets are becoming increasingly important. The self-organizing map (SOM), an artificial neural network technique based on unsupervised learning, is an effective tool of feature extraction (Kohonen 1982; 2001) that preserves the topological relationships of the input data. In the current study, SOM has been utilized for aerosol optical depth (AOD) and precipitation rate (PR) projections based on the Community Climate System Model version 4 (CCSM4) and worst case scenarios of aerosol emissions (Lamarque *et al.*, 2010, 2011) over the region.

Atmospheric aerosol projections form the basis on decision making particularly on climate change and their influence on air quality, health and agriculture. For example, over East Africa i.e. Nairobi (1°S, 36°E), Mbita (0°S, 34°E), Mau Forest (0.0-0.6°S; 35.1-35.7°E), Malindi (2°S, 40°E), Mount Kilimanjaro (3°S, 37°E) and Kampala (0°N, 32.1°E), aerosol source regions are greatly influenced either anthropogenically or naturally (Mabasi, 2009; Fairman *et al.*, 2011; Makokha and Angeyo, 2013; NEMA, 2013; Mutugi and Kiiru, 2015). In the previous case, fine mode aerosols over urban, industrialized and densely populated regions (Nairobi and Kampala) are mainly due to gas-to particle conversion mechanism of aerosols (fossil fuel, industrial-vehicular emissions, biomass and refuse burning) (Vliet and Kinney, 2007). Biomass burning and deforestation activities have impacted highly on the regional aerosol loading that modulate climate e.g. the disappearance of Mount Kilimanjaro glaciers (Fairman *et al.*, 2011) and the Mau Forest Complex. Moreover, the latter case constitutes mainly coarse mode aerosols from dust loading, farming and maritime conditions i.e. sea salt and spray aerosols (Malindi), Lake-land air mass exchange (Mbita) and long distance transport of aerosols from the Arabian Peninsula desert via Monsoon winds over Malindi (Makokha and Angeyo, 2013). The most recent trend analyses over East Africa indicate an increase in both AOD and absorption aerosol index (AAI) while a decline was noted in the Angstrom exponent (AE) during the same study period (Boiyo *et al.*, 2016). There is a need therefore to understand the future evolution of aerosol characteristics and their impacts on future regional climate.

A number of methods have been used in climate and precipitation projections over East Africa. To start with, Souverijns *et al.* (2016) utilized a classification of circulation patterns in an ensemble of Regional Climate Model (RCM) to project a 23 % future change over East Africa. This RCM studies projected an increase in annual precipitation over areas located near the equator (Otieno and Anyah, 2013; Buontempo *et al.*, 2015) which contrasts the current drying trend. Other studies by Cook and Vizzy (2013) projected a decline in precipitation based on a RCM with 90-km horizontal resolution on a large domain that is attributable to increasing greenhouse gases over the region.

As a tool for pattern recognition and classification, the SOM analysis is in widespread use across a number of disciplines among them climate research (Liu *et al.*, 2006; Liu and Weisberg, 2011). SOM has been utilized in quantifying various changes in meteorological variables and further reveal the underlying mechanisms driving the change (Cassano *et al.*, 2007; Natasa and Jennifer, 2012). Additionally, SOM can also be utilized to extract obscure climate diagnostic information from large multidimensional datasets as demonstrated by Natasa and Jennifer (2012). A study by Lamarque *et al.* (2010) indicates a reasonable agreement between total AERONET AOD observations with that of the Community Atmosphere Model 4 (CAM4) simulations at $\lambda = 550$ nm, hence, their utility in projection studies. Shindell *et al.* (2013) used the CAM4 atmospheric aerosol concentration dataset and demonstrated that it captures total AOD trends of 1980–2000 well over the areas of high aerosol emissions (e.g., Europe, eastern North America and southern and eastern Asia).

In the current study, CAM4 was utilized in simulating both AOD and PR over East Africa (Gent *et al.*, 2011; Neale *et al.*, 2011). The first case of simulations started from 2000 to 2014 while the second case was from 2015 to 2030. In the first instance, an initial validation was implemented between MODIS and CAM4 simulates for AOD and TRMM and CAM4 simulates for PR as a future proof of quality check. Subsequently, the second scenario allows for the utilization of CAM4 AOD and PR simulates together with the SOM algorithm in projecting their future evolution characteristics from 2015 to 2030 based on worst case scenarios of aerosol emissions (Lamarque *et al.*, 2010; 2011).

2. Methodology

Level-3 MODIS gridded atmosphere monthly global product ‘MOD08_M3’ AOD (at 550 nm) at spatial resolution of $1^\circ \times 1^\circ$ (Ichoku, *et al.*, 2004) and TRMM Microwave Imager Precipitation Profile L3 1 month data at the spatial resolution of $0.5^\circ \times 0.5^\circ$ V7 (TRMM_3A12), were retrieved from 2000 to 2014 over each of the study sites. The details of how the two monthly products are organized and utilized in the proposed SOM algorithm are shown in section 2.1.

2.1. Self-Organizing Map (SOM)

SOM comprise of a two layered network that organizes the input patterns to a topological structure represented by its neurons while preserving the relations between different patterns. To achieve this, the following topology and training rules of Kohonen mapping were applied for clustering, classification, and feature extraction in MODIS spectral images from 2000 to 2014.

1. The training of the network is implemented by presenting data vectors x to the input layer of the network whose connection weight vectors m_i of all competitive neurons i are chosen random values. If N is the dimension of the satellite spectral data, we chose N input neurons and define the Euclidean distance (d_i) between x and m_i as:

$$d_i = \|x - m_i\| = \sqrt{\sum_{j=1}^N (x_j - m_{ij})^2} \quad (1)$$

and determine the activated neuron c with $d_c = \min_i \{d_i\}$.

2. Updating of the weights m_{ij} that are associated to the neurons is only performed within the proximity ($i \in N_c(t)$) of c that reduces with the training time t and $N_c(t)$ is the winning neuron. The process of updating is implemented via the equation 2b where $a(t)$ represents a time dependent learning rate:

$$m_{ij}^{t+1} = m_{ij}^t + \Delta m_{ij}^{(t)} \quad (2a)$$

$$\Delta m_{ij}^{(t)} = \begin{cases} a(t)(x_j - m_{ij}^{(t)}), & \text{if neuron } i \in N_c(t) \\ 0, \dots \dots & \text{otherwise} \end{cases} \quad (2b)$$

$$a(t) = a_o \left(1 - \frac{t}{T}\right), \quad t \in [0, \dots \dots T] \quad (2c)$$

The time dependent neighborhood is updated according to:

$$d(t) = d_o \left(1 - \frac{t}{T}\right), \quad t \in [0, \dots \dots T] \quad (2d)$$

It is therefore important to note that the network performs two features during the training, which are strongly related to both clustering and classification of the MODIS and TRMM spectral data over the region. These are:

1. A separation, i.e. cluster analysis of the presented data by mean vectors m_i that are associated as weights to the neurons.
2. A topological ordering of the competitive neurons in such a way that neighboring neurons in the layer represent similar clusters in multidimensional space and thus dimensionality reduction.

Based on Cassano *et al.* (2007), we have formulated a method that separates factors contributing to temporal change in both AOD and PR into:

- a) Portion caused by a change in the frequency of occurrence (FO) of monthly AOD and PR maps in a node.
- b) Portion due to a change in the node mean value in both AOD and PR.

c) Portion as a result of the combination of the two effects.

The stated factors that contribute to the temporal changes in both AOD and PR, we can define the following sets of equations:

$$\Delta\tau = \sum_{i=1}^N \{(\tau_i + \Delta\tau_i)(f_i + \Delta f_i) - \tau_i f_i\} \quad (3a)$$

$$\Delta\alpha = \sum_{i=1}^N \{(\alpha_i + \Delta\alpha_i)(f_i + \Delta f_i) - \alpha_i f_i\} \quad (3b)$$

where $\Delta\tau$ and $\Delta\alpha$ are the total change in AOD and PR between two different time periods, τ_i and α_i are the node average variables in both AOD and PR respectively in the initial period. f_i is the FO of monthly maps in node i during the initial period while Δf_i is the change in FO for node i between the two periods of interest. Additionally, $\Delta\tau_i$ and $\Delta\alpha_i$ are the changes in both AOD and PR node average variables between the two periods while N is the total number of nodes in each SOM map over each site of study. Expanding Equations 3a and b, we have:

$$\Delta\tau = \sum_{i=1}^N (\tau_i \Delta f_i + f_i \Delta\tau_i + \Delta\tau_i \Delta f_i) \quad (4a)$$

$$\Delta\alpha = \sum_{i=1}^N (\alpha_i \Delta f_i + f_i \Delta\alpha_i + \Delta\alpha_i \Delta f_i) \quad (4b)$$

The first terms in Equations 4a and b i.e. $\tau_i \Delta f_i$ and $\alpha_i \Delta f_i$ relate changes in monthly AOD and PR fields respectively to changes in the FO of aerosol optical patterns over each study site. These patterns show a portion of the total change owing to the shifts in the frequencies with which monthly AOD and PR fields reside in the patterns depicted in the SOM. A change in AOD and PR distribution represents a change in aerosol characteristics which directly and indirectly alter regional climate (Charlson *et al.*, 1992; IPCC, 2013) and further affect the air quality, hence, referred to as a dynamic factor. The second term in Equations 4a and b i.e. $f_i \Delta\tau_i$ and $f_i \Delta\alpha_i$ relates the temporal evolution in AOD and PR fields respectively averaged over all months belonging to a give node. In the case of aerosol optical properties, such changes are caused by thermodynamic effects such as local air circulation, urban heat islands effects, among others. The third term in Equation 1 represents the contribution from the interaction of both changing pattern frequency and the node averaged variable for both AOD and PR. This term tends to be small as compared to the other two. For any input data matrix of n -variables (spatial variability) and m -observations (samples) (temporal variability) the iterative SOM training procedure is as detailed elsewhere (Crane and Hewitson, 2003). To enhance the SOM capabilities in the prediction of both AOD and PR, simulations from the CAM4 were utilized as described in Section 2.2.

2.2. Community Atmosphere Model 4 (CAM4) Simulations

The CAM4 is the sixth generation atmospheric general circulation models (AGCMs) developed by the atmospheric modeling community in collaboration with the National Center for Atmospheric Research (NCAR). For detailed descriptions of CAM4 see Neale *et al.* (2011). CAM4 has been designed to produce simulations with reasonable accuracy for various dynamical cores and horizontal resolution of $0.9^\circ \times 1.25^\circ$ (Boyle and Klein, 2010). It is important to note that CAM4 includes the direct and semi-direct effects of aerosols while missing out on the aerosol first indirect effect (Twomey *et al.*, 1984).

3. Results and Discussions

Before actual projections in both AOD and PR, it is necessary first to determine the Root Mean Square Error (RMSE) between measured and CAM4 simulations to cross validate the CAM4 simulations against MODIS and TRMM measurements over the study sites from 2000 to 2014. The values of both RMSE and R^2 informs us on the reliability of CAM4 simulates for AOD and PR projections by 2030 over the region. Figure 1 shows that the CAM4 simulated AOD are lower as compared to MODIS retrievals as a result of tropical precipitation in the online simulation as detailed in Lamarque *et al.* (2011). Despite this observation, AOD CAM4 simulations correlate positively against MODIS measurements with RMSE = 0.04 and $R^2 = 0.58$ over Nairobi (Figure 1a). On the contrary, CAM4 overestimates the PR as compared the TRMM actual measurements over Nairobi. The overestimation is attributed to the dependence of quality precipitation simulations from CAM4 to the choice of the horizontal resolution used in the retrieval of PR over Nairobi (Boyle and Klein, 2010) (Figure 1b). From Figure 1 and based on RMSE = 0.08 and $R^2 = 0.52$, it is noticeable that AOD and PR CAM4 simulate values can be used to project the irregional evolution with satisfactory uncertainty by 2030.

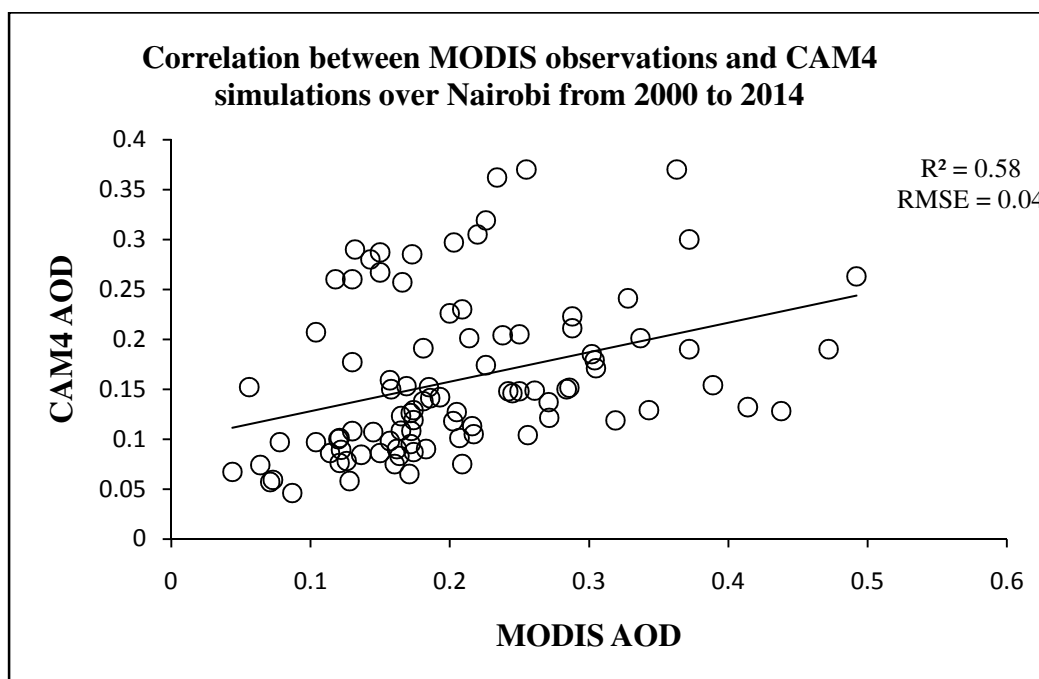


Figure 1a: Cross validation of AOD MODIS retrievals and CAM4 simulations at $\lambda = 550$ nm

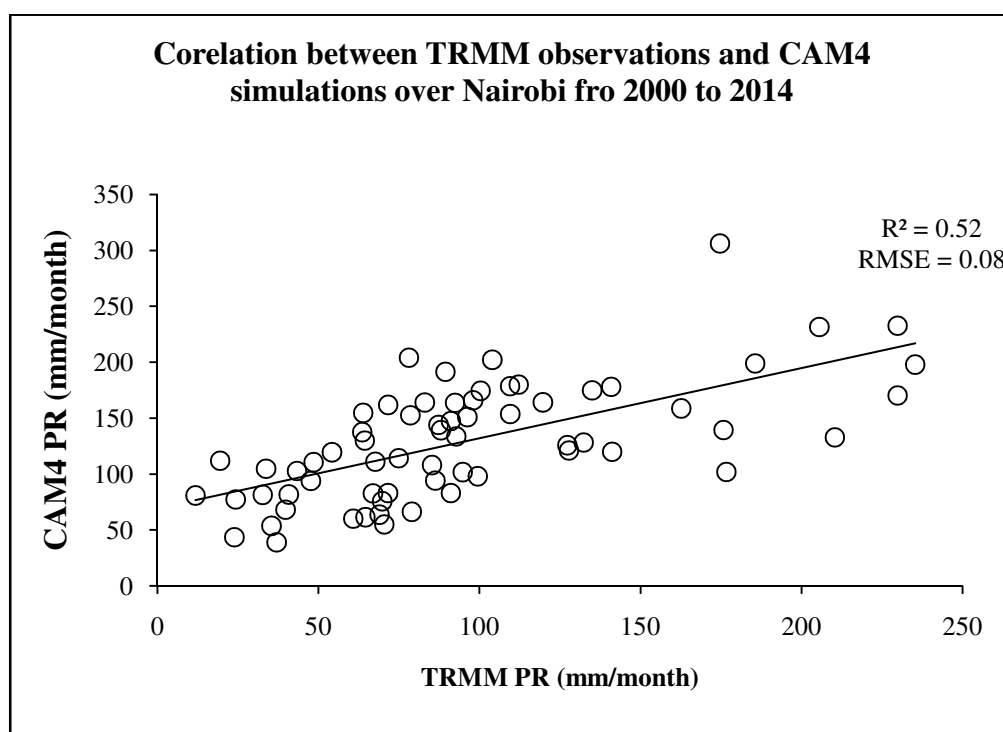


Figure 1b: Cross validation of PR TRMM retrievals and CAM4 simulations.

Error analysis between CAM4 simulations and MODIS measurements shows a close match where $R^2 > 0.58$ and RMSE 0.04 (for AOD) while $R^2 > 0.52$ and RMSE 0.08 (for PR) over Nairobi. The low values of the RMSE shown in Figure 1 enhance the confidence in utilizing AOD and PR simulations from CAM4 in environmental related studies. Details of R^2 and RMSE for the remaining study sites are shown in Table 1. Table 1 details the RMSE distributions between the modeled AOD and PR (CAM4 simulated retrievals) and MODIS and TRMM retrieved values.

Site of Study	RMSE in AOD (R^2)	RMSE in PR (R^2)
Nairobi	0.04 (0.58)	0.08 (0.52)
Mbita	0.065 (0.73)	0.026 (0.78)
Malindi	0.06 (0.83)	0.091 (0.40)
Mau Forest	0.014 (0.67)	0.021 (0.48)
Mt Kilimanjaro	0.032 (0.59)	0.036 (0.57)
Kampala	0.029 (0.63)	0.034 (0.56)

Table 1: RMSE between the simulated CAM4 and MODIS and TRMM observed AOD and PR study sites

High RMSE for simulated CAM4 and TRMM values over the study sites may be attributed to the dependence of quality precipitation simulations from CAM4 to the choice of the horizontal resolution used in the retrieval of PR over the site (Boyle and Klein, 2010). On the other hand, cross validation between simulated AOD from CAM4 and that retrieved from MODIS relatively low RMSE values (0.014-0.065) signifying an appreciable agreement in the two techniques. Therefore, the utilization simulated CAM4 AOD and PR in quest to project their future characteristics is possible due to the low RMSE and high R^2 (see Table 1).

3.1. Projections of Aerosol Optical Depth and Precipitation Rate

Essentially, several means were utilized to display the SOM array in both AOD and PR over each study site; these are histogram, correlation analysis and Sammon map. Based on these results, it is clear that SOM classifies both AOD and PR into 20 clusters based on the amount of PR (mm per month) over each site. Of significance to note are the clusters with zero FO (y-axis of the histogram) i.e. there is no monthly AOD or PR values that were classified into the corresponding cluster e.g. PR classification over Malindi for clusters 10-19 (see Figure 2c, plane 3 x 1). Figure 2 shows a SOM array for both AOD and PR over the study sites during the study period.

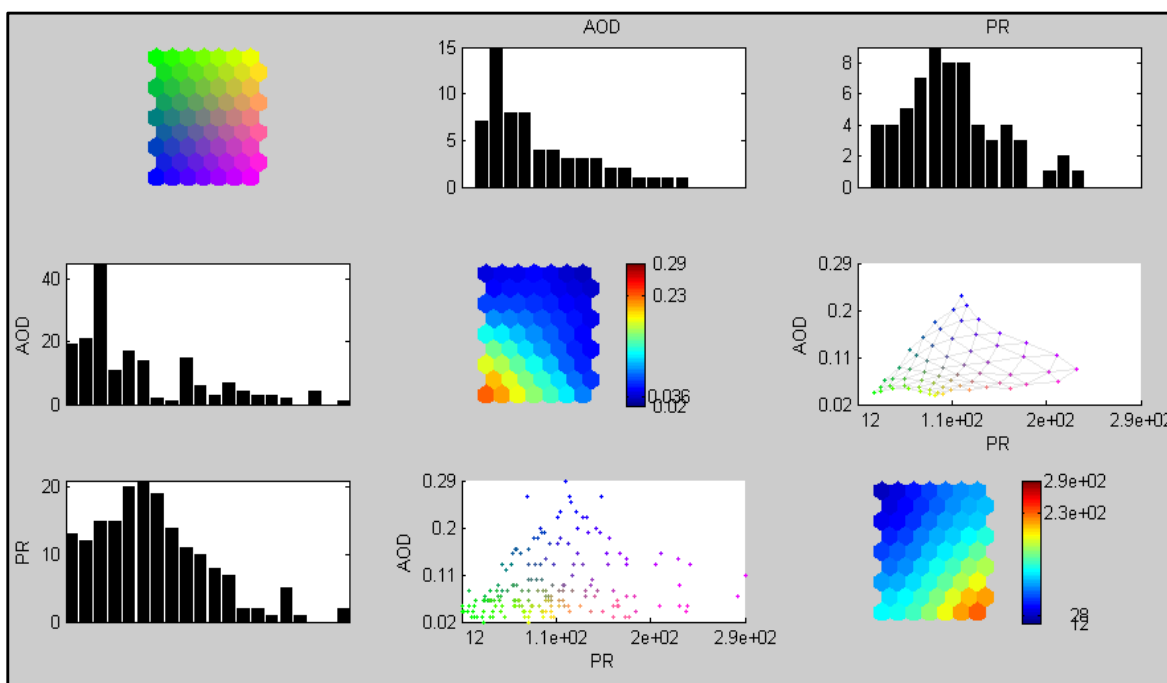


Figure 2a: SOM array for both AOD and PR over Nairobi.

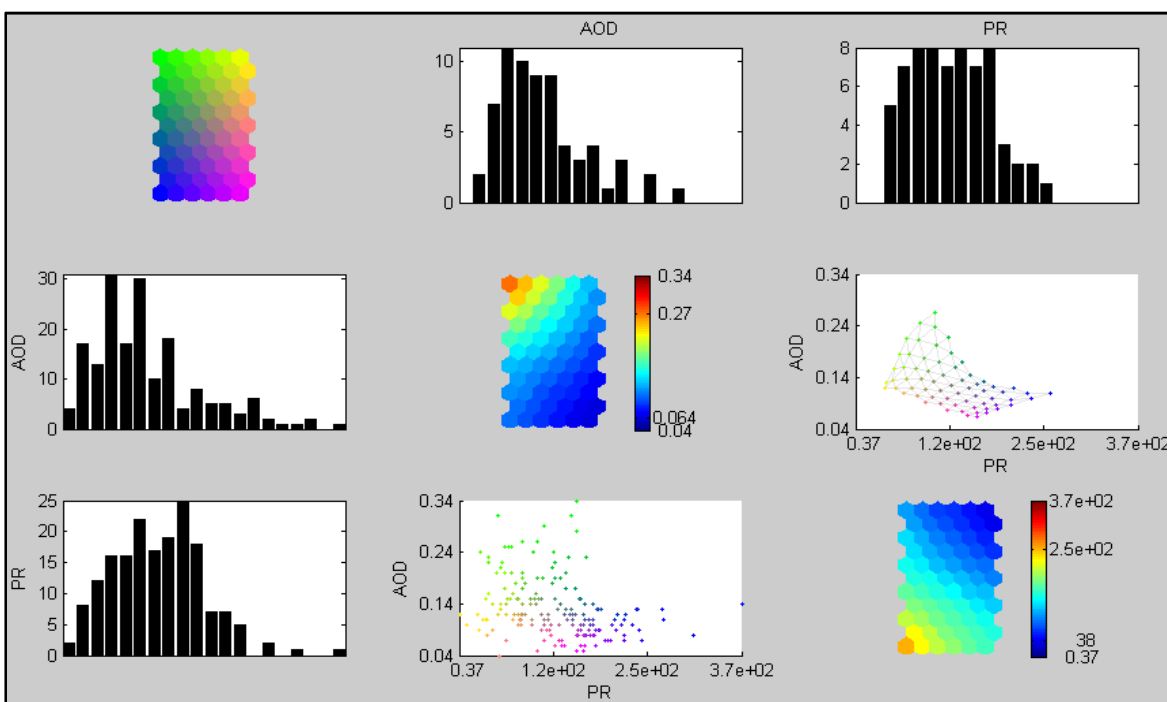


Figure 2b: SOM array for both AOD and PR over Mbita.

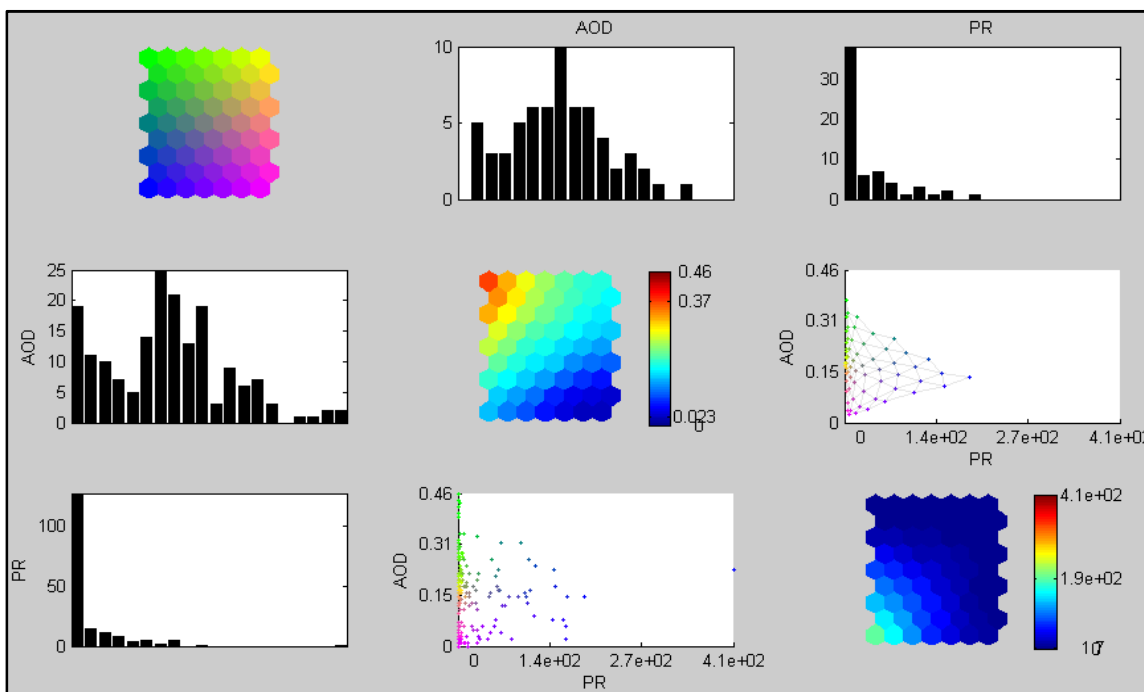


Figure 2c: SOM array for both AOD and PR over Malindi.

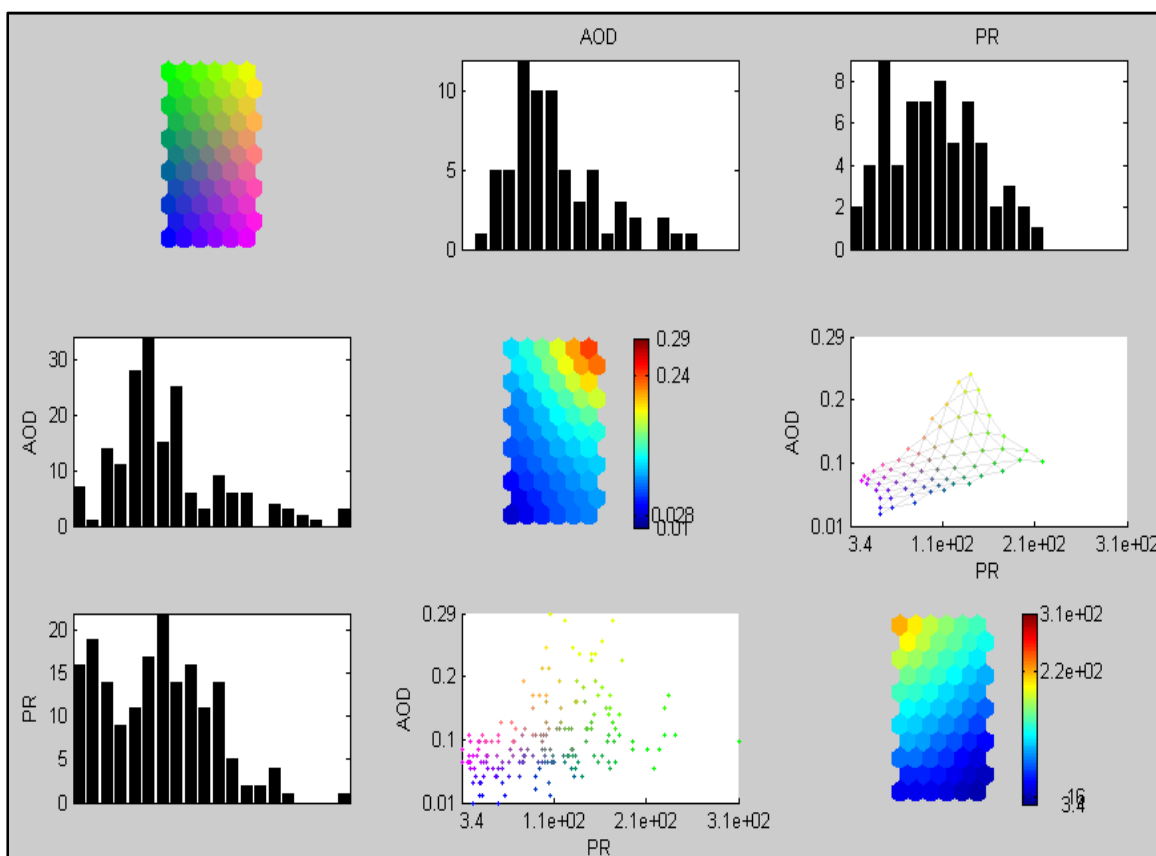


Figure 2d: SOM array for both AOD and PR over Mau Forest Complex.

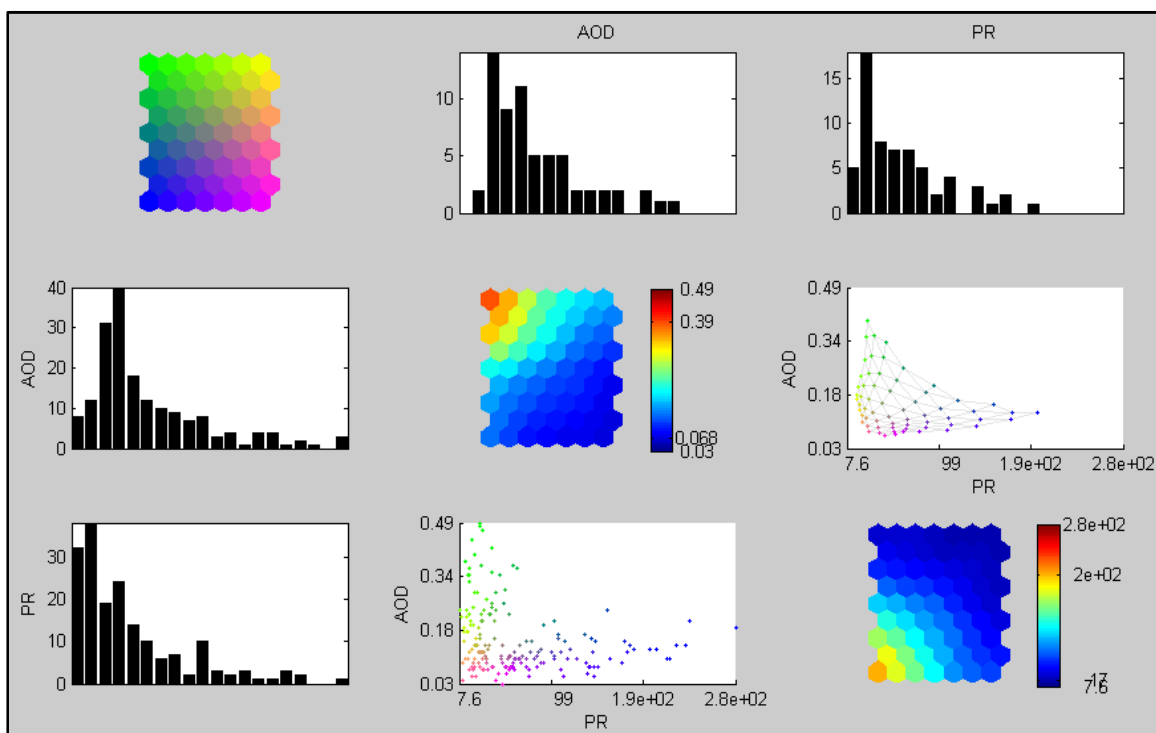


Figure 2e: SOM array for both AOD and PR over Mount Kilimanjaro.

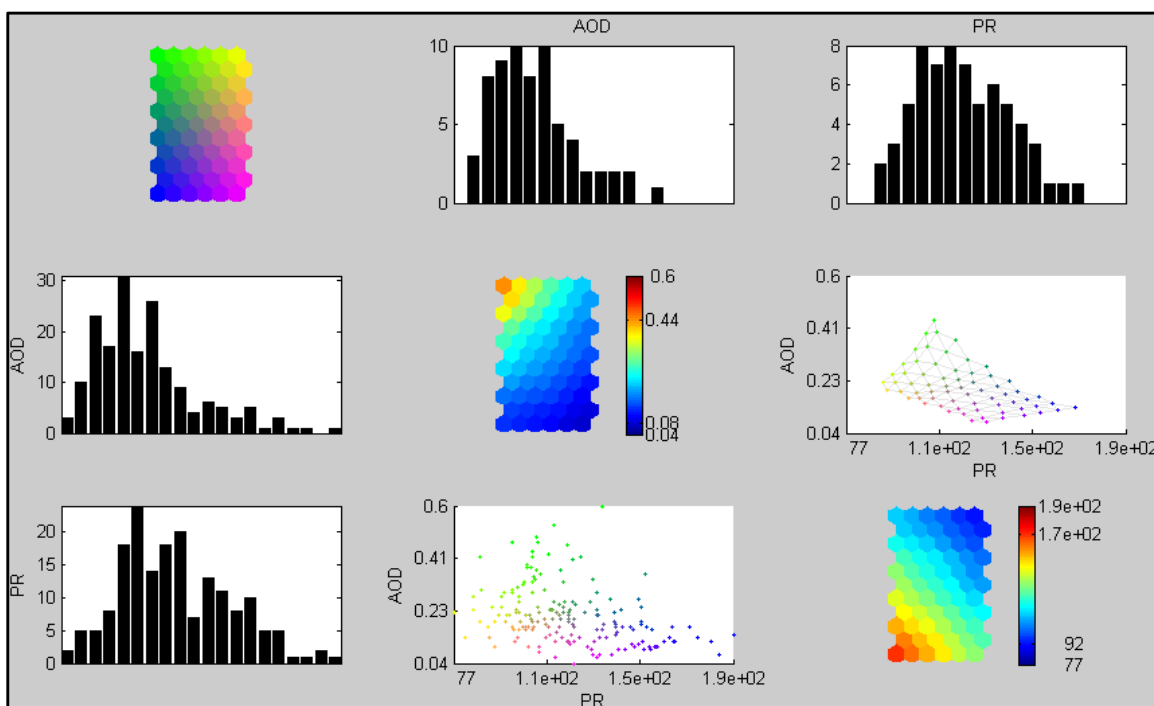


Figure 2f: SOM array for both AOD and PR over Kampala.

In the present study we focused on AOD and PR projections over East Africa by 2030. Figure 3 displays the projected percentage change in both AOD and PR based on the CAM4 simulated values by 2030 using SOM technique as described in Sections 2.1 and 2.2.

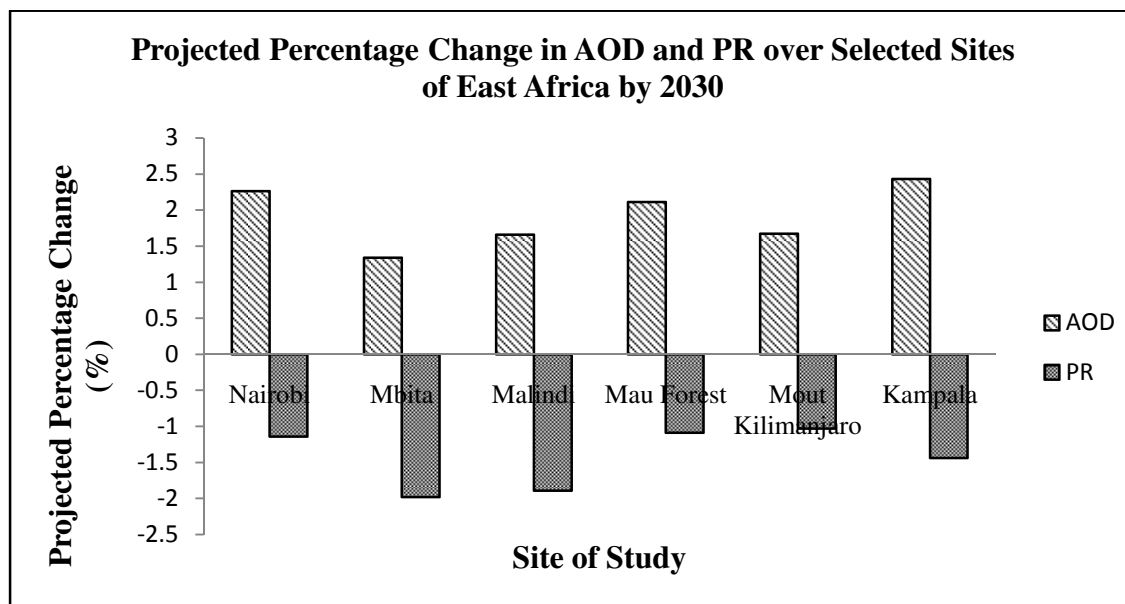


Figure 3: Projected percentage change in both AOD and PR over East Africa based on SOM and simulated CAM4 by 2030

Total AOD is projected to increase between 1.34-2.43 % while PR is projected to decrease between 1.03-1.98 % respectively. The projected increase in AOD may be attributed to continual increase in anthropogenic influence of aerosol characteristics over the region i.e. vehicular and industrial emissions, deforestation, and biomass burning among others (Vliet and Kinney, 2007; Fairman *et al.*, 2011; Makokha and Angeyo, 2013; Ngaina and Mutai, 2013; Ngaina *et al.*, 2014). The projected decrease in PR over the region is associated to the dependence of Lake-land air mass over Mbita. The projected decrease in PR over the sites will lead to adverse effects such as hampering food production therefore impacting negatively on regional food security. These projections are on assumption that if no mitigation efforts are implemented to minimize both anthropogenic and natural aerosol modulators over East Africa, then aerosol loading increase is imminent.

4. Conclusions

Improved techniques in climate projections and scenarios informs on decision making relating to climate change adaptation. This not only enhances the preparedness of key policy making institutions on climate change effects but also allows for advancing mitigation efforts beforehand. In the present study, utilization of CAM4 simulates i.e. AOD and PR in the projection of their future evolutionary characteristics over the region is appropriate as noted from the low RMSE and high R^2 . Utilization of the proposed SOM algorithm indicated a diminishing PR as projected by the SOM algorithm over the region which may impact negatively on food production by 2030. Increasing aerosol burdens as projected by the SOM algorithm calls for urgent planning by all stakeholders concerning food security in the region and minimizing on the increasing anthropogenic burden on aerosol loading mainly through biomass and refuse burning.

5. Acknowledgements

This work was supported by the National Council for Science and Technology Grant funded by the Government of Kenya (NCST/ST&I/RCD/4TH call PhD/201). The authors wish to thank the Giovanni online data system that is developed and maintained by the NASA Goddard Earth Science Distributed Active Archive (NASA GES DISC) from which the MODIS AOD and TRMM PR data utilized in the study was obtained. I also acknowledge the support of the African Spectral Imaging Network (AFSIN) through funding the first author to travel to a conference on Multispectral imaging in Senegal.

6. References

- i. Boiyo, R., Kumar, K.R., Zhao, T., and Bao, Y. (2016). Climatological analysis of aerosol optical properties over East Africa observed from space-borne sensors during 2001–2015. *Atmospheric Environment*, **152**, 298-313.
- ii. Boyle, J. and Klein, S. A. (2010). Impact of horizontal resolution on climate model forecasts of tropical precipitation and diabatic heating for the TWP-ICE period, *J. Geophys. Res.*, **115**: D23113, doi: 10.1029/2010JD014262.
- iii. Buontempo, C., Mathison, C. J. R., Williams, K., Wang, C. and McSweeney, C. (2015). An ensemble climate projection for Africa *Clim. Dyn.* **44**: 2097–118.
- iv. Cassano, J. J., Uotila, P., Lynch, A. H. and Cassano, E. N. (2007). Predicted changes in synoptic forcing of net precipitation in large Arctic river basins during the 21st century, *J. Geophys. Res.*, **112**: G04S49, doi:10.1029/2006JG000332.
- v. Charlson, R. J., Schwartz, S. E., Hales, J. M., Cess, R. D., Coakley, J. A., Hansen, J. E. and Hofmann, D. J. (1992). Climate forcing by anthropogenic aerosols. *Science*, **255**: 423-430.
- vi. Cook, K. H. and Vizy, E. (2013). Projected changes in East African rain seasons. *Journal of Climate Change*. **26**:5831-5948.
- vii. Crane, R. G. and B. C. Hewitson (2003), Clustering and upscaling of station precipitation records to regional patterns using self-organizing maps (SOMs), *Clim. Res.*, **25**: 95–107.
- viii. De Graaf, M., Tilstra, L. G., Aben, I. and Stammes, P. (2010). Satellite observations of the seasonal cycles of absorbing aerosols in Africa related to the monsoon rainfall, 1995–2008. *Atmos. Environ.* **44**: 1274–1283.
- ix. Fairman, J.G., Nair, U.S., Christopher, S.A., Mölg, T. (2011). Land use change impacts on regional climate over Kilimanjaro. *J. Geophys. Res. Atmospheres* **116**: D03110. doi:10.1029/2010JD014712.
- x. Gatari, M. J., Boman, J. and Annemarie, W. (2009). Characterization of aerosol particles at an industrial background site in Nairobi, Kenya. *X-ray Spectrom.* **38**: 37-44.
- xi. Gatebe, C. K., Tyson, P. D., Annegarn, H., Piketh, S. and Helas, G. (1999). A seasonal air transport climatology for Kenya, *J. Geophys. Res.* **104 (D12)**: 14237-14244.
- xii. Gent, P. R., Danabasoglu, G., Donner, L. J., Holland, M. M., Hunke, E. C., Jayne, S. R., Lawrence, D. M., Neale, R. B., Rasch, P. J., Vertenstein, M., Worley, P. H., Yang, Z.-L. and Zhang, M. (2011). The community climate system model version 4, *J. Climate*, **24**: 4973–4991, doi:10.1175/2011JCLI4083.1.
- xiii. Ichoku, C., Kaufman, Y.J., Remmer, L.A. and Levy R. (2004). Global aerosol remote sensing from MODIS, *Adv. Space Res.* **34(4)**: 820-827.
- xiv. IPCC, 2013: Climate Change 2013: The Physical Science Basis. Contribution of Working Group I to the Fifth Assessment Report of the Intergovernmental Panel on Climate Change [Stocker, T. F., D. Qin, G.-K. Plattner, M. Tignor, S. K. Allen, J. Boschung, A. Nauels, Y. Xia, V. Bex and P. M. Midgley (Eds.)]. Cambridge University Press, Cambridge, United Kingdom And New York, NY, USA, 1535. Doi: 10.1017/CBO9781107415324.
- xv. Kohonen, T. (1982). Self-organized information of topologically correct features maps. *Biol. Cybernetics*, **43**: 59–69.
- xvi. Kohonen, T. (2001). *Self-Organizing Maps*. Springer-Verlag, ISBN 3-540-67921-9, New York, Berlin, Heidelberg.
- xvii. Lamarque, J. F., Bond, T. C., Eyring, V., Granier, C., Heil, A., Klimont, Z., Lee, D., Liousse, C., Mieville, A., Owen, B., Schultz, M. G., Shindell, D., Smith, S. J., Stehfest, E., Van Aardenne, J., Cooper, O. R., Kainuma, M., Mahowald, N., McConnell, J. R., Naik, V., Riahi, K., and van Vuuren, D. P. (2010). Historical (1850–2000) gridded anthropogenic and biomass burning emissions of reactive gases and aerosols: methodology and application, *Atmos. Chem. Phys.*, **10**: 7017–7039, doi:10.5194/acp-10-7017-2010.
- xviii. Lamarque, J. F., Kyle, G. P., Meinshausen, M., Riahi, K., Smith, S. J., van Vuuren, D. P., Conley, A., and Vitt, F. (2011). Global and regional evolution of short-lived radiatively-active gases and aerosols in the representative concentration pathways, *Climatic Change*, **109**: 191–912, doi:10.1007/s10584-011-0155-0.
- xix. Lau, K. M., Kim, M. K. and Kim, K. M. (2006). Asian monsoon anomalies induced by aerosol direct forcing: The role of the Tibetan Plateau. *Clim. Dyn.* **26**:855–864.

- xx. Liu, Y. and Weisberg, R. (2005). Patterns of ocean current variability on the West Florida Shelf using the self-organizing map, *Journal of Geophysical Research*, **110**: C06003, doi:10.1029/2004JC002786, ISSN 0148-0227
- xxi. Liu, Y. and Weisberg, R. H. (2011). A Review of Self-Organizing Map Applications in Meteorology and Oceanography, *Self Organizing Maps - Applications and Novel Algorithm Design*, Josphat Igadwa Mwasiagi (Ed.), ISBN: 978-953-307-546-4, InTech, DOI: 10.5772/13146.
- xxii. Mabasi, T. (2009). Assessing the impacts, vulnerability, mitigation, and adaptation to climate change in Kampala city. Kampala, Uganda: Fifth Urban Research Symposium 2009.
- xxiii. Makokha, J.W. and Angeyo, H. K. (2013). Investigation of Radiative Characteristics of the Kenyan Atmosphere due to Aerosols Using Sun Spectrophotometry Measurements and the COART Model. *Aerosol Air Qual. Res.* **13**:201-208.
- xxiv. Makokha, J. W., J. N. Kimani and H. K. Angeyo (2012). Estimation of radiative forcing due to aerosols over selected sites in Kenya. *J. Meteorol. Rel. Sci.*, **6**: 3-13.
- xxv. Mutugi, M and Kiiru, W. (2015). Biodiversity, local resource, National heritage, Regional concern and global impact: The case of Mau Forest, Kenya. *ESJ.*, **1**:681-691.
- xxvi. Natasa S. and Jennifer F. (2012). *Self-Organizing Maps: A Powerful Tool for the Atmospheric Sciences, Applications of Self-Organizing Maps*, Dr. Magnus Johnsson (Ed.), ISBN: 978-953-51-0862-7, InTech, DOI: 10.5772/54299.
- xxvii. National Environmental Management Authority, Kenya (NEMA). Mau at a glance. NEMA Report, 2013.
- xxviii. Neale, R. B., Richter, J. H., Conley, A. J., Park, S., Lauritzen, P. H., Gettelman, A., Williamson, D. L., Rasch, P. J., Vavrus, S. J., Taylor, M. A., Collins, W. D., Zhang, M., and Lin, S. (2011). Description of the NCAR Community Atmosphere Model (CAM4), Tech. Rep. NCAR/TN+STR, National Center for Atmospheric Research, Boulder, CO, 194 pp., available on-line at <http://www.cesm.ucar.edu/models/ccsm4.0/cam>.
- xxix. Ngaina, J. K. and Mutai, B. K. (2013). Observational evidence of climate change on extreme events over East Africa. *Glob. Meteorol.* **2**(1):6-12.
- xxx. Ngaina, J.N., Mutai, B.K., Ininda, J.M. and Muthama, J.N. (2014). Monitoring spatial-temporal variability of aerosol over Kenya. *Ethiop. J. Environ. Stud. Manag.* **7**: 244–252.
- xxxi. Otieno, V. O. and Anyah, R. O. (2013). CMIP5 simulated climate conditions of the Greater Horn of Africa (GHA): II. Projected climate. *Clim. Dyn.* **41**: 2099–2113.
- xxxii. Shindell, D. T., Lamarque, J.-F., Schulz, M., Flanner, M., Jiao, C., Chin, M., Young, P. J., Lee, Y. H., Rotstayn, L., Mahowald, N., Milly, G., Faluvegi, G., Balkanski, Y., Collins, W. J., Conley, A. J., Dalsoren, S., Easter, R., Ghan, S., Horowitz, L., Liu, X., Myhre, G., Nagashima, T., Naik, V., Rumbold, S. T., Skeie, R., Sudo, K., Szopa, S., Takemura, T., Voulgarakis, A., Yoon, J.-H. and Lo, F. (2013). Radiative forcing in the ACCMIP historical and future climate simulations, *Atmos. Chem. Phys.*, **13**, 2939–2974, doi:10.5194/acp-13-2939-2013.
- xxxiii. Souverijns, N., Thiery, W., Demuzere, M. and Van Lipzig, N. P. M. (2016). Drivers of future changes in East African precipitation. *Environ. Res. Lett.* **11**: 114011. DOI: <https://doi.org/10.1088/1748-9326/11/11/114011>.
- xxxiv. Twomey, S. A., Piegrass, M., and Wolfe, T. L. (1984). An assessment of the impact of pollution on global cloud albedo, *Tellus*, **36**: 356–366.
- xxxv. Vliet, E.D.S. van and Kinney, P.L. (2007). Impacts of roadway emissions on urban particulate matter concentrations in sub-Saharan Africa: new evidence from Nairobi, Kenya. *Environ. Res. Lett.* **2**: 045028. doi:10.1088/1748-9326/2/4/045028